ACS APPLIED MATERIALS & INTERFACES

www.acsami.org

Research Article

Nanoporous Carbon Materials as Solid Contacts for Microneedle Ion-Selective Sensors

Yevedzo Chipangura, Maria Komal, Vilma S. M. Brandao, Christopher Sedmak, Jung Suk Choi, Sarah L. Swisher, Philippe Bühlmann,* and Andreas Stein*

Cite This: *ACS Appl. Mater. Interfaces* 2024, 16, 44428–44439

Read Online

ACCESS | Metrics & More | Article Recommendations | Supporting Information

ABSTRACT: Continuous sensing of biomarkers, such as potassium ions or pH, in wearable patches requires miniaturization of ion-selective sensor electrodes. Such miniaturization can be achieved by using nanostructured carbon materials as solid contacts in microneedle-based ion-selective and reference electrodes. Here we compare three carbon materials as solid contacts: colloid-imprinted mesoporous (CIM) carbon microparticles with ~24−28 nm mesopores, mesoporous carbon nanospheres with 3−9 nm mesopores, and Super P carbon black nanoparticles without internal porosity but with textural mesoporosity in particle aggregates. We compare the effects of carbon architecture and composition on specific capacitance of the material, on the ability to incorporate ion-selective membrane components in the pores, and on sensor performance. Functioning K^+ and H^+ ion-selective electrodes and reference electrodes were obtained with gold-coated stainless-steel microneedles using all three types of carbon. The sensors gave near-Nernstian responses in clinically relevant concentration ranges, were free of potentially detrimental water layers, and showed no response to O_2. They all exhibited sufficiently low long-term potential drift values to permit calibration-free, continuous operation for close to 1 day. In spite of the different specific capacitances and pore architecture of the three types of carbon, no significant difference in potential stability for K^+ ion sensing was observed between electrodes that used each material. In the observed drift values, factors other than the carbon solid contact are likely to play a role, too. However, for pH sensing, electrodes with CIM as a carbon solid contact, which had the highest specific capacitance and best access to the pores, exhibited better long-term stability than electrodes with the other carbon materials.

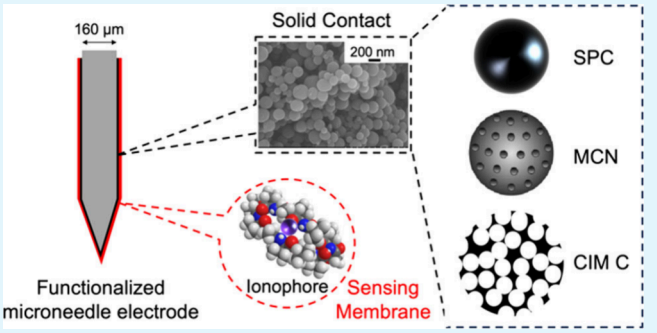

KEYWORDS: *microneedle sensor, ion-selective electrode, nanostructured carbon solid contact, sensor miniaturization, pore architecture, ionophore*

INTRODUCTION

Miniaturized wearable and implantable sensors are promising to transform healthcare and personal monitoring due to their potential to provide real-time and continuous tracking of biomarkers. Compared to conventional sensing methods that require drawing of blood and may be painful, wearable sensors can be minimally invasive or noninvasive if they measure analytes in biofluids such as interstitial fluid, sweat, saliva or tears, instead of blood.[1−7] In particular, interstitial fluid has a high correlation to blood plasma concentrations of several of the most common analytes of interest.[1]

Potentiometric ionophore-based sensing with ion-selective electrodes (ISEs)[8−14] is currently used to make over a billion measurements per year in clinical and industrial settings.[15,16] Conventional ISEs are highly developed and reliable, however, because of the inner filling solution used for transduction, they are difficult to miniaturize and require frequent recalibration. To address this limitation, the inner filling solution can be replaced with a solid contact material.[16−19] The solid contact is sandwiched between the electrode substrate and the ion-selective membrane, and it serves to convert the charge carrier from ions to electrons. For this role, nanostructured carbon materials offer various advantages. They possess high specific surface areas that are required for a large double-layer capacitance at the interface of the ion-selective membrane and the solid contact, leading to a high stability of the measured potential. Their hydrophobicity avoids the formation of a water layer that can produce unstable signals, and they are suitable for miniaturized electrodes.

Materials such as conducting polymers have been studied as solid contacts; however, their redox potentials are not well-

Received: May 9, 2024
Revised: August 6, 2024
Accepted: August 7, 2024
Published: August 15, 2024

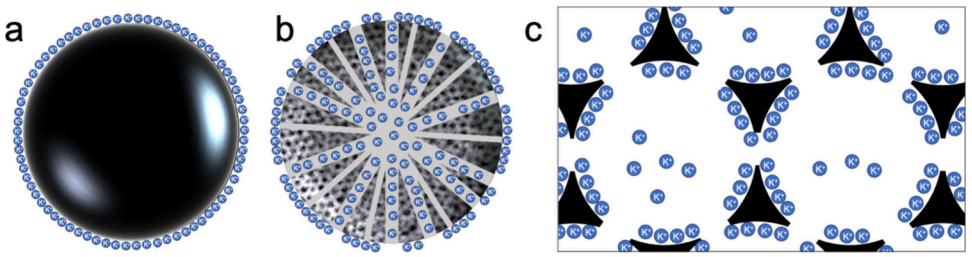

Figure 1. Schematic diagram illustrating accessibility of surfaces to ISM components on the external and/or internal surfaces of (a) nonporous carbon particles (SPC), (b) carbon nanoparticles with small mesopores (MCN), and (c) carbon particles with large mesopores (CIM carbon). The blue circles represent the ionophore−K^+ complexes that contribute to the double-layer capacitance. In (b) some mesopores are not accessible because they are too small for this complex to enter.

defined, which can promote side reactions that increase potential drift.[20] Carbon materials with different architectures have also been investigated as solid contacts, including carbon black,[21−23] nanographite,[24] carbon nanotubes,[8,9,24−26] graphene,[27] porous carbon nanospheres,[28,29] 3-dimensionally ordered macroporous (3DOM) carbon,[30] and colloid-imprinted mesoporous (CIM) carbon.[16,31] 3DOM carbon and CIM carbon are both templated materials, where porosity is introduced by sacrificial polymer spheres or silica spheres, respectively. 3DOM carbon is a nanostructured solid contact with interconnected pores (∼350 nm). Its bicontinuous structure with continuous electron-conducting walls and continuous void space that can be filled with ion-containing sensing membrane material makes it a good ion-to-electron transducer, with a reported drift of 11.7 μV h^{-1}.[32] One limitation of 3DOM carbon prepared in monolithic form is that it restricts the possible extent of sensor miniaturization.[30,32] However, CIM carbon can also be made in powder form, making it suitable for surface coating, and it has been applied in paper-based electrodes[33] and on polymeric flexible electrode substrates.[34] The particle size of CIM carbon can be reduced by sonication to form particles smaller than a few micrometers in diameter that are suitable for coating inks. It has a high mesopore surface area required for a good ion-to-electron transducer, and a low content of redox impurities. CIM carbon also has an interconnected pore structure, with large mesopores (∼24−28 nm) that should be accessible to the ion-selective membrane (ISM) components, such as polyvinyl chloride (PVC), plasticizer (e.g., dioctyl sebacate, DOS), ionophore (e.g., valinomycin for K^+ or tridodecylamine for H^+), and ionic sites (e.g., tetrakis(pentafluorophenyl)borate). Potassium ISEs based on CIM carbon have been reported to exhibit a potential drift as low as 1.3 μV h^{-1},[16,35] which means they can be used for several weeks without needing recalibration. For shorter-term continuous use of wearable sensors, such as during surgery or a short hospital stay, potential drift requirements are less stringent. According to U.S. Federal Regulation (Clinical Laboratory Improvement Act, 42 CFR 493.931), as of July 2024, the acceptable error in measurement of potassium ion concentration within the clinically relevant range (3.4−5.3 mM) is ±0.3 mM[36] or 1.4 mV. This would limit potential drifts for K^+-ISEs to better than 59 μV h^{-1} if continuous measurements are performed over 1 day, or 177 μV h^{-1} if measurements are done over a shift of 8 h before the sensors are recalibrated. Similarly, the acceptable error for pH measurements is ±0.04 or 2.4 mV.[36] A drift of 100 μV h^{-1} would allow calibration-free operation of pH-ISEs for 1 day.

For the implementation of wearable sensors, microneedle-based ISEs have been developed, including some on flexible patches. Different types of microneedles have been used as electrodes for wearable sensors,[37] including those prepared by micromachining,[38] 3D printing,[11] or soft lithography;[13] and the needles can be hollow[10,11] or solid.[8] Acupuncture microneedles have also been used due to their low cost and commercial availability. Microneedle ISEs have been reported for sensing of different analytes and biomarkers such K^+,[8−10] Na^+,[9,10] pH,[9,11−13] Cl^-,[9] and CO_2.[12] For example, Crespo et al. describe a wearable solid state potentiometric microneedle patch for K^+ sensing using functionalized multiwalled carbon nanotubes as solid contact and observed a potential drift of 0.35 ± 0.28 mV h^{-1}.[8] A multi-ion pH and carbonate sensor using functionalized multiwalled carbon nanotubes as solid contact was reported with drifts of 1.6 mV h^{-1} and 2.1 mV h^{-1}, respectively.[12]

At this point, the impact of the specific architecture of carbon-based solid contact materials on critical parameters of microneedle electrodes — response slope, linear range, standard potential, and long-term potential drift — has not yet been systematically studied. The objective of this study is to evaluate the suitability of nanoporous carbon materials as solid contacts for microneedle-based ion-selective sensors and to investigate the effects of materials architecture on these parameters. We compare three types of carbon materials as the solid contact: CIM carbon with ∼24−28 nm mesopores,[16] mesoporous carbon nanospheres (MCN) prepared using block copolymer templates to produce 3−9 nm mesopores,[39] and the commercial carbon black Super P carbon (SPC), which consists of nonporous particles. MCNs are viable solid contacts for miniaturized ISEs,[28,29] including microneedle electrodes, because they can be readily synthesized with sufficiently small particle size (a few hundred nm) to produce a uniform solid contact coating on small electrodes. SPC consists of relatively uniform carbon nanoparticles 50−100 nm in diameter. SPC has only external surfaces, and mesoporosity arises from textural mesopores within particle aggregates with a specific surface area of 65 m^2/g.

We hypothesize that in the porous solid contacts, only pore surfaces that are accessible to the ionophore, ionic sites, and ion-selective membrane components contribute to the double-layer capacitance that enables the conversion of ion to electron conduction.[24] Thus, one would expect that potential drift depends not only on the total surface area of the solid contact but also on its pore architecture. Most of the surface in CIM carbon with large mesopores and the external surface of nonporous SPC should be accessible to all the ISM components used in this study (Figure 1). However, in

https://doi.org/10.1021/acsami.4c07683
ACS Appl. Mater. Interfaces 2024, 16, 44428−44439

MCN, the smaller mesopores may not be accessible to some ISM components. Here we first show the effects of pore architecture on specific capacitance and on infiltration with membrane components (PVC, plasticizer). We then demonstrate that all three of these carbon materials can be used as solid contacts on acupuncture microneedles to make K^+ and pH ISEs and reference electrodes that are suitable for measurements in clinically relevant concentration ranges with sufficiently low drift for continuous monitoring over 8−24 h before recalibration. We focus on K^+ and H^+ sensing because any imbalance of either of these ions consistently correlates with poor clinical outcomes.[40] Continuous real-time monitoring of these ions would enable clinicians to probe disease progression and potentially mitigate mortality risk.[40]

EXPERIMENTAL SECTION

Materials. Formalin aqueous solution (37 wt % formaldehyde) was purchased from J.T. Baker. Phenol (99 wt %), NaOH (97 wt %), KOH (≥85%, pellets), KCl (99.0−100.5%), the nonionic copolymer surfactant Pluronic F-127, high molecular weight poly(vinyl chloride) (PVC), ammonium tetrakis(3-chlorophenyl)borate, dioctyl sebacate (DOS), valinomycin (potassium ionophore I), tetrahydrofuran (THF) (99.9%, inhibitor-free), cyclohexanone, acetonitrile, lithium acetate (LiOAc, 99.95%), and Ludox AS-40 colloidal silica (40 wt % suspension in H_2O) were purchased from Sigma-Aldrich. The plasticizer *ortho*-nitrophenyl octyl ether (*o*-NPOE, 98%) was purchased from Aaron Chemicals. Tridodecylamine and tetrabutylammonium perchlorate were purchased from Tokyo Chemical Industry, ethanol (EtOH, anhydrous, 200 proof) from Decon Laboratories, mesophase pitch from Mitsubishi Gas Chemicals, 1-hexanethiol (96%) from Acros Organics, and 1-dodecyl-3-methylimidazolium bis(trifluoromethylsulfonyl)imide from Ionic Liquid Technologies. Anhydrous inhibitor-free tetrahydrofuran (THF) was passed through basic alumina before use. All other chemicals were used without further purification. Super P carbon (SPC) was purchased from MTI Corporation. The syntheses of MCN and CIM carbon are described in the Supporting Information. Stainless steel acupuncture needles with a diameter of 160 μm and 13 mm length, and gold plated surgical stainless steel acupuncture needles with a diameter of 160 μm and 25 mm length (Tai Chi 24 K gold plated) were purchased from Massage Warehouse (massagewarehouse.com). Deionized water was produced on-site using a Milli-Q PLUS reagent grade water system to a minimum resistivity of 18.2 MΩ·cm. N_2 gas and N_2/H_2 (95%/5%) gas were purchased from Airgas.

Preparation of Carbon Ink. The carbon inks were prepared by mixing PVC with DOS plasticizer and THF and stirring the mixture for 24 h to fully dissolve PVC before adding carbon. For MCN and CIM C, we used 60 mg carbon, 30 mg PVC, 30 mg DOS, and 0.5 mL THF. SPC ink was prepared using 180 mg SPC, 90 mg PVC, 90 mg DOS, and 3 mL THF. The carbon inks were bath sonicated for 30 min to break down any chunks present and yield better dispersions of carbon particles. The carbon inks for pH measurements were prepared with the same compositions, except for using 30 mg of *o*-NPOE plasticizer instead of DOS.

Preparation of Ion-Selective Membrane (ISM) and Reference Membrane Solutions. Potassium-ion-sensing membranes were prepared by dissolving 132 mg PVC (polymer matrix), 264 mg DOS, 4 mg valinomycin, and 0.85 mg ammonium tetrakis(3-chlorophenyl) borate in 2 mL THF. The ionophore:ionic site ratio was 2:1. pH-sensing membranes were prepared by dissolving 132 mg PVC, 264 mg *o*-NPOE, 0.82 mg of the ionophore tridodecylamine, and 0.38 mg ammonium tetrakis(3-chlorophenyl) borate in 2 mL THF. The molecular ratio of ionophore to ionic site was 2:1. Reference membrane solutions were prepared by dissolving 120 mg PVC, 120 mg DOS, and 60 mg of the ionic liquid 1-dodecyl-3-methylimidazolium bis(trifluoromethylsulfonyl)imide ($[C_{12}mim^+][NTf_2^-]$) in 2 mL THF.

Fabrication of Microneedle ISEs. Gold-coated microneedles were rinsed with a 50/50 v/v ethanol/water mixture and dried in air. To ensure a hydrophobic surface, these needles were coated with a self-assembled monolayer formed by immersion into 1 mM 1-hexanethiol in ethanol for 24 h. The needles were rinsed then with ethanol and dried in air. To apply the carbon coating, each needle was dipped into the carbon ink three times to ensure full coverage, especially on the tip, allowing solvent to evaporate after each immersion into the ink. When the tip was not fully coated with carbon, the electrodes did not function well and suffered from water layer formation as shown in Figure S9. The needles were left to dry in air for 3 h. Then they were coated with the ISM or reference membrane solution twice, waiting for 3 h between coats. The needles were left to dry for 24 h.

Materials Characterization. The particle sizes and morphologies of the carbon materials were analyzed using scanning electron microscopy (SEM). The materials were coated with a 5 nm thick Pt layer and imaged using a Hitachi SU8230 with a field emission gun operating at 5.0 kV. The particle size distribution was determined manually via the ImageJ program using SEM images of spheres after hydrogen treatment. Nitrogen sorption measurements were carried out using a Quantachrome Autosorb iQ2 analyzer. Samples were outgassed at 120 °C for 12 h under vacuum (1 mTorr) before analysis. Nitrogen sorption isotherms were analyzed by the Brunauer−Emmett−Teller method to determine surface areas. A quenched solid density functional theory (QSDFT) model for N_2 isotherms at 77 K on carbon (slit/cylindrical/spherical pore, QSDFT adsorption branch model) was used to calculate DFT pore size distributions, DFT pore volumes, and DFT surface areas. CHN analyses of the carbon materials were carried out by Atlantic Microlabs (Norcross, GA). X-ray photoelectron spectroscopy (XPS) was performed using a PHI 5000 VersaProbe III Photoelectron Spectrometer with Al Kα X-ray radiation. The C_{1s} peak at 284.4 eV was used to calibrate other XPS peak positions.

Electrochemical Measurements. The electrode potentials were measured using a 16-channel potentiometer that was controlled by EMF Suite software (Lawson Labs, Malvern, PA). Potentials were measured against a conventional free-flow, double-junction reference electrode (DX200, Mettler Toledo, Switzerland), in which AgCl saturated 3.0 M KCl was used as the inner reference electrolyte and 1.0 M LiOAc was used as the bridge electrolyte. The Henderson equation was used to correct the measured emf values for the liquid junction potential of the double junction reference electrode,[41] and activity coefficients were calculated using a two-parameter Debye−Huckel approximation.[42] The resistances of membrane coated microneedles were measured using the shunt method.[43] Long-term stability measurements were measured relative to an electrolytically coated Ag/AgCl wire in 1 mM KCl.

Water Layer Test. For K^+-sensing electrodes, a water layer test was performed by exposing the electrodes to 0.1 M KCl solution, then to 0.1 M NaCl (interfering ion) solution, and then again to 0.1 M KCl, while measuring the electrode potentials.[30] For pH sensing electrodes, the water layer test was performed by exposing the electrodes to 0.1 M phosphate buffer solution of pH 7.1, then to 0.1 M NaOH (interfering ion) solution, and then again to 0.1 M phosphate buffer, while measuring the electrode potentials.

Selectivity. The selectivities of the ISEs were measured using the fixed interference method (FIM).[34,44,45] For K^+-ISEs, the electrodes were placed in a solution containing 1 M NaCl and 10^{-7} M KCl, and concentrations of KCl were adjusted by adding aliquots from a concentrated KCl solution to obtain a calibration curve. For pH-ISEs, the electrodes were placed in a solution containing 1 M NaCl and 0.1 M phosphate buffer, and the pH was adjusted using NaOH or HCl solutions.

Oxygen and Carbon Dioxide Sensitivity Test. Sensitivity to oxygen and carbon dioxide was measured by first bubbling an inert gas (argon for K^+-ISEs, nitrogen for pH-ISEs) through 1 mM KCl solution and measuring the potential vs time of the microneedle ISEs, then bubbling oxygen, or carbon dioxide through the solution and recording the potential vs time for 30 min.

https://doi.org/10.1021/acsami.4c07683
ACS Appl. Mater. Interfaces 2024, 16, 44428−44439

RESULTS AND DISCUSSION

Characterization of the Carbon Materials. A sufficiently small carbon particle size is needed to create uniform solid contact coatings. The microneedles used in this work have diameters of 160 μm, and the particle size of solid contact carbon materials should be less than a few micrometers to enable uniform coatings of the needles with a solid contact layer. The particle size, shape, and morphology of the three carbon materials were analyzed using SEM images as shown in Figure 2. Mesoporous carbon nanospheres synthesized in this work have particle sizes ranging from 50 to 350 nm, with a mean distribution around 170 nm (Figure S1a,b). CIM carbon (Figure 2b and S2) has uniformly sized and interconnected mesopores. The particles of CIM carbon were reduced to <5 μm diameter via probe sonication (Figure S1c,d). The resulting particles had irregular shapes and formed larger agglomerates (Figure S2). SPC has particle sizes between 50 and 100 nm, as shown in Figure 1c, making it useful for carbon ink preparation without needing further size reduction.

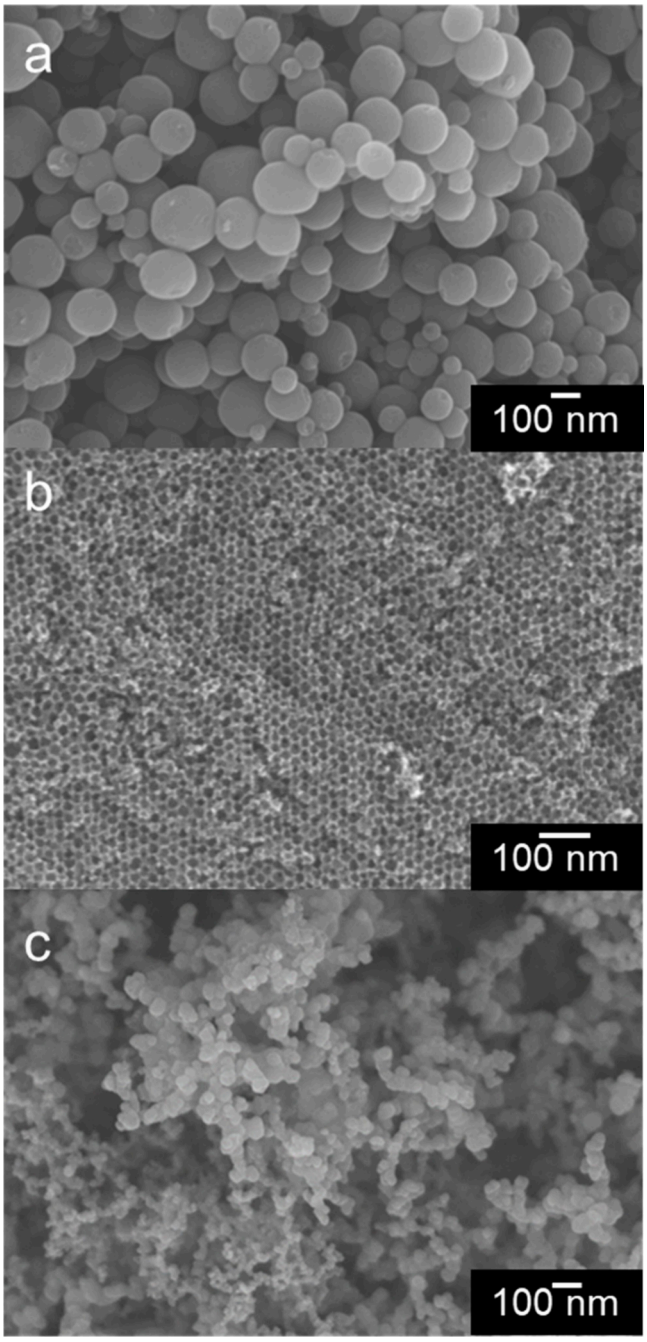

Figure 2. SEM images of (a) MCN, (b) CIM carbon, and (c) SPC. See also Figures S1 and S2 in the Suppporting Information.

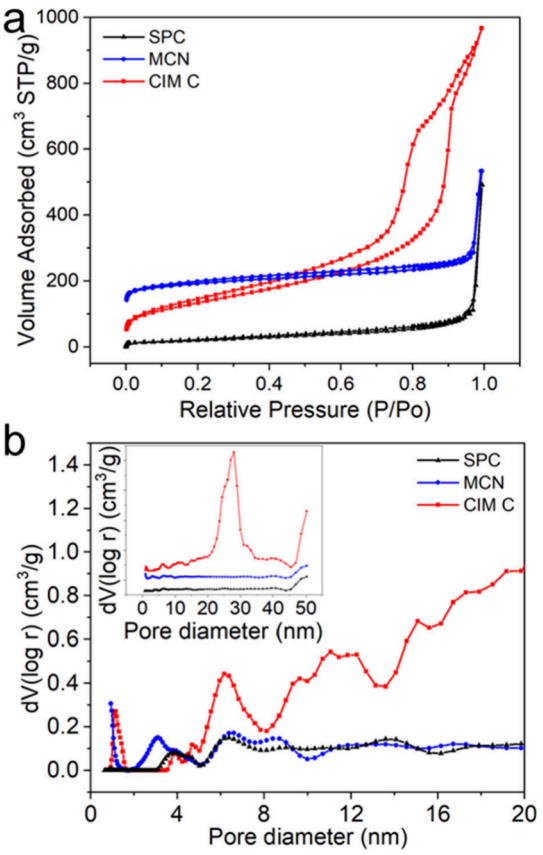

Figure 3. (a) N_2 adsorption−desorption isotherms, and (b) pore size distributions for CIM C (red), MCN (blue), and SPC (black). The inset shows an extended range of the pore size distribution up to 50 nm.

The pore structure of the carbon materials was determined using N_2 physisorption isotherms. For MCN and CIM carbon, a knee is observed at low relative pressure, indicating the presence of some micropores (<2 nm in diameter), while for all three carbons, the steep rise in adsorbed volume at high relative pressure (P/P_0 > 0.9) indicates textural porosity (interparticle pores between agglomerated carbon particles). The isotherm of MCN is pseudotype I, with a narrow H1 hysteresis loop,[11,12] as shown in Figure 3a, indicating small mesopores in the range of 3−9 nm. CIM carbon shows a typical type IVa isotherm with a hysteresis between the adsorption and desorption curves, associated with large mesopores between 24 and 28 nm (Figure 3b). The type I isotherm of SPC indicates that these carbon nanoparticles are nonporous, only forming textural mesopores. The corresponding textural data (pore diameters, pore volumes, specific surface areas) are provided in Table 1. CIM carbon has the largest mesopore volume, mesopore surface area, and overall pore volume, followed by MCN, then SPC. MCN has the highest specific surface area, but much of that surface area is related to micropores.

https://doi.org/10.1021/acsami.4c07683
ACS Appl. Mater. Interfaces 2024, 16, 44428−44439

Table 1. Pore Diameters, Pore Volumes, Specific Surface Areas, Specific Capacitance Values Measured by Cyclic Voltammetry (CV) and Chronopotentiometry (CP), and Calculated Amounts of Each Carbon Material Required to Achieve a Drift Low Enough to Enable Calibration-Free Measurements over 1 Week for MCN, CIM Carbon, and SPC

	MCN	CIM carbon	SPC
particle size (nm)	50−350	<5 μm diameter	50−100
DFT pore diameter (nm)	3−9	24	textural mesopores
DFT pore volume (cm^3/g)	0.40	1.3	0.15
	micropores: 0.24	micropores: 0.04	all external
	mesopores: 0.13	mesopores: 1.18	
	external: ∼0.02	external: ∼0.08	
BET specific surface area (m^2/g)	800	430	65
DFT specific surface area (m^2/g)	micropores: 742	micropores: 60	65
	mesopore: 88	mesopores: ∼360	all external
	external: ∼3	external: ∼9	
CV capacitance (F/g)	2.9 ± 0.5 (n = 3)	23 ± 3 (n = 3)	2.5 ± 0.1 (n = 3)
CP capacitance (F/g)	3.4 ± 0.7 (n = 3)	23 ± 2 (n = 3)	2.5 ± 0.0 (n = 3)
material required for low drift (μg) (K^+-ISE)	7.7	0.9	8.6
material required for low drift (μg) (pH-ISE)	4.6	0.6	5.1

Table 2. Elemental Analyses of MCN, CIM C, and SPC[a]

	C (wt %)	H (wt %)	N (wt %)	O (wt %)
MCN	97.64 (96.55)[c]	0.34	0.00	3.45[c]
CIM C	96.32 (96.30)[c]	0.61	0.00	3.20.[c]
SPC	99.86	0.00	0.00	n.d.[d]
CIM C[b]	96.02	0.46	0.00	0.43
3DOM C[b]	92.95	0.27	0.00	2.13

[a]CHN determined by combustion analysis by Atlantic Microlab. [b]Published values reported in ref 16 using titration data to determine oxygen groups. [c]Determined by XPS analysis. See Figure S3. [d]n.d. = not determined.

For carbon materials used as solid contacts in ISEs, the purity of the carbon is important. In particular, redox active groups, such as those arising from oxygen-containing or nitrogen-containing functional groups, must be avoided. For this reason, the processing of MCN and CIM carbon involved a reduction step, in which the materials were exposed to hydrogen at 900 °C to remove any oxygen groups that were introduced from the precursor (MCN synthesis) or during template extraction (CIM carbon). Elemental analysis (Table 2) showed that the CIM carbon CHN composition was similar to that reported previously for a CIM carbon solid contact for ISEs[16] and that MCN had an even higher carbon content and should, therefore, also be suitable for ISE applications. The higher measured oxygen content of the CIM carbon sample compared to the previously reported material is likely due to the different analysis technique used; XPS is a technique that is only able to analyze the surface of carbon particles while the titration analysis also reflects the surface chemistry of accessible pore surfaces within carbon particles. It appears that the oxygen to carbon ratio is higher on external particles surfaces. SPC, which has been optimized as a commercial conducting agent for lithium-ion batteries has the highest carbon content, with no significant impurities.

Infiltration of the Carbon Materials with Membrane Components. To determine how infiltration of ISM components into the pores of the carbon materials is limited by pore architecture, samples of nanostructured carbon were prepared with different fractional filling of pores with PVC and the DOS plasticizer (see the Supporting Information). We used the densities of PVC or 2:1 DOS/PVC mixtures and the measured total pore volume of each carbon material to calculate the masses of DOS and PVC needed to fill the pores completely (100% filling) or partially (20 or 30%). In the case of SPC, which consists of nonporous carbon black particles with mesoporosity arising only from interparticle spaces, upon addition of PVC and DOS, the specific surface area is reduced slightly as a polymer layer forms on the particle surface and effective particle sizes are enlarged (see Table S2). Some textural mesoporosity remains between the coated particles.

After infiltration of CIM carbon with the polymer components (30% filling or 100% filling), the mesopore volume decreases as the amounts of PVC and DOS increase, and the very small fractional volume of micropores (3%) becomes fully blocked. At the same time, the peak in the mesopore size distribution shifts to lower values, consistent with the formation of a coating on the mesopore surface, which could also block entry of adsorbent gas to micropores. For infiltrations with PVC/DOS mixtures, the decrease in mesopore volume is relatively close to that expected if mostly the smaller DOS molecule entered the mesopores. However, partial penetration of mesopores by PVC chains is also possible, as indicated by the 63% reduction in mesopore volume by plasticizer-free PVC. Approximate diameters are 1.7 nm for DOS, 1.9 nm for the K^+−valinomycin complex, 1.9 nm for the H^+ ionophore tridodecylamine, and 1.0 nm for the ionic site species tetrakis(pentafluorophenyl)borate.[46] Given that the ionophore and ionic site dimensions are not larger than those of DOS, we can assume that those components would also be able to enter these mesopores. Even with a hypothetical 100% filling of all particle pores, some structural mesoporosity remains in the CIM carbon−polymer composites, and an excess of PVC/DOS is required to eliminate all the mesopore volume observed by N_2 gas sorption analysis.

The situation is more complex for MCN, which has a wider distribution of mesopore sizes between about 3 and 9 nm, besides larger textural mesopores between particles. Although the surface area is relatively large, the majority of it comes from micropores. These micropores are fully blocked after exposure to the polymer. The BET surface area is reduced to values one would expect for nonporous spheres having diameters close to those of the MCN particles. When MCN is loaded with PVC or a PVC/DOS mixture, the mesopore volume is essentially unchanged or even increases, probably due to introduction of additional pores in the polymeric phase of the resulting composite material. From this we conclude that PVC and DOS do not penetrate MCN particles to a significant extent. The PVC/DOS mixture coats the particles, also blocking mesopores between particles. Given that the size of the K^+ ionophore valinomycin is similar to that of DOS, these observations suggest that K^+ complexes of valinomycin can only assemble in an electrical double layer on the outside of

https://doi.org/10.1021/acsami.4c07683
ACS Appl. Mater. Interfaces 2024, 16, 44428−44439

Table 3. Electrical and Response Parameters of Microneedle Based ISEs and REs

electrode type		MCN	CIM C	SPC
K^+	response (mV/decade)	60.0 ± 0.5	58.0 ± 1.6	58.3 ± 0.5
	E^0 (mV)	340 ± 31	138 ± 18	361 ± 71
	detection limit (M)	$10^{-5.5\pm0.1}$	$10^{-5.5\pm0.1}$	$10^{-5.4\pm0.0}$
	response time (s)	14 ± 0	7 ± 0	12 ± 2
	resistance (MΩ)	3.5 ± 0.6	2.7 ± 0.6	2.1 ± 0.2
	log $K^{pot}_{K^+,Na^+}$	−4.2 ± 0.1	−4.1 ± 0.1	−4.3 ± 0.1
	drift (μV h^{-1}) (4−10 days)[a]	−127 ± 229	55 ± 139	−12 ± 60
	number of electrodes (n)	3	3	3
H^+	response (mV/decade)	−54.7 ± 4.1	−56.9 ± 0.5	−55.9 ± 3.1
	E^0 (mV)	339 ± 35	504 ± 9	413 ± 23
	response time (s)	9 ± 3	7 ± 3	10 ± 2
	resistance (MΩ)	0.7 ± 0.1	0.5 ± 1	0.3 ± 0.0
	log $K^{pot}_{H^+,Na^+}$	−11.8 ± 0.2	−11.9 ± 0.1	−11.7 ± 0.1
	drift (μV h^{-1}) (4−10 days)[a]	95 ± 176	10 ± 20	186 ± 13
	number of electrodes (n)	3	3	3
RE	response (mV/decade)	−0.11 ± 0.56	−0.64 ± 0.72	−0.22 ± 0.35
	E^0 (mV)	−12 ± 114	4 ± 41	−34 ± 112
	resistance (MΩ)	4.0 ± 1	1.5 ± 0.4	3.5 ± 0.8
	drift (μV h^{-1}) (4−10 days)[a]	−67 ± 96	109 ± 60	−125 ± 90
	number of electrodes (n)	5	5	5
μneedle K^+ vs μneedle RE	response (mV/decade)	62.1 ± 0.6	57.9 ± 1.1	59.5 ± 0.4
	E^0 (mV)	331 ± 24	122 ± 30	250 ± 18
	number of electrodes (n)	4	3	2

[a]Drift was calculated from 4 to 10 days to account for conditioning during the first 4 days.

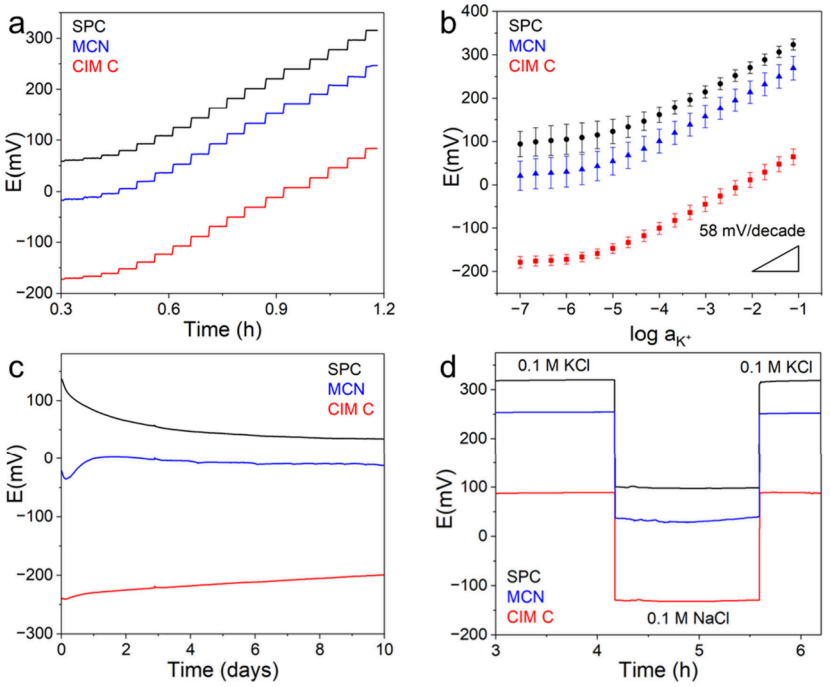

Figure 4. (a) Dynamic responses, (b) calibration curves, (c) long-term drift and (d) water layer test for microneedle ISEs made using SPC (black), MCN (blue) and CIM C (red) as solid contact together with a K^+ ion-selective membrane. (a), (b), and (d) were measured vs a double junction Ag/AgCl reference electrode, whereas (c) was measured vs an electrolytically coated Ag/AgCl wire. The response analyses and water layer tests were carried out after the long-term drift measurements.

the MCN particles, similar to the situation for SPC. Larger mesopores would be required in MCN-type particles to ensure penetration of ionophore complexes and ionic site species.

Capacitance of the Carbon Solid Contact Materials. The solid contact functions as an ion-to-electron transducer, and in the case of nanoporous or nanostructured carbon materials also plays a role in mitigating drift of the measured potential from the small current that flows through the sensor during measurement as a result of the finite input impedance of the potentiometer ($\Delta E/\Delta t = i/C$, where E = potential, t = time, i = current, C = capacitance).[18] Thus, if sensor drift is limited by the input impedance of the potentiometer, one

https://doi.org/10.1021/acsami.4c07683
ACS Appl. Mater. Interfaces 2024, 16, 44428−44439

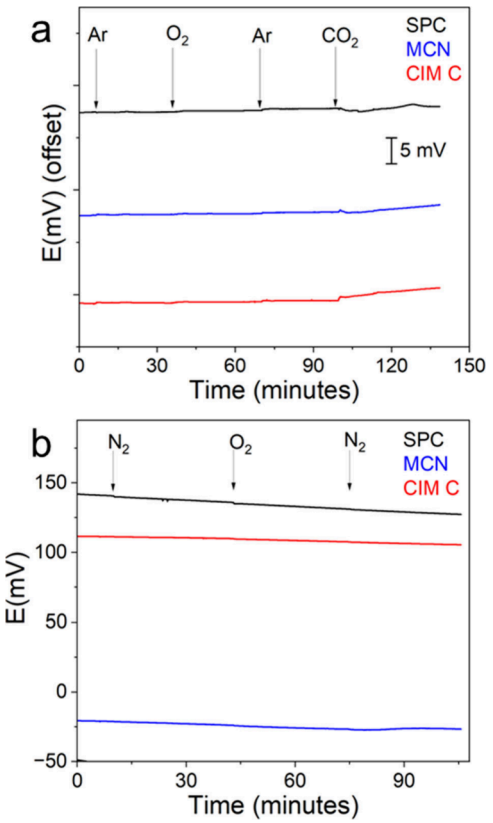

Figure 5. (a) Effect of oxygen and carbon dioxide on the potential stability in 1 mM KCl solution of microneedle based K^+-ISEs with CIM C (red), MCN (blue) and SPC (black) as solid contact. (b) Effect of oxygen on pH-ISEs in 0.1 M phosphate buffer at pH 7 with CIM C (red), MCN (blue) and SPC (black) as solid contact. The drift in potential observed here is likely due to ion exchange, given that the sensitivity test was carried out immediately after the water layer test.

would expect to observe less drift with a larger capacitance of the solid contact. The specific capacitance values of the three carbon materials were determined by cyclic voltammetry and chronopotentiometry (Tables 1 and S3, Figure S5). The values obtained by both methods are comparable. Even though MCN has by far the largest overall specific surface area, its specific capacitance is nearly an order of magnitude smaller than that of CIM carbon. This difference can be attributed to the fact that most of the surface area in CIM carbon arises from large mesopores that are easily accessible to electrolyte ions at the time scale of the measurements, whereas the largest fraction of surface area in MCN arises from micropores that are too transport-limiting for electrolyte ions. In the case of SPC, the particle surface is external, with an area of 65 m^2/g, slightly lower than the mesopore surface area of MCN (88 m^2/g), so that the specific capacitance of SPC was also slightly lower than that of MCN.

Microneedle Electrode Fabrication. Acupuncture microneedles are used in traditional Chinese medicine to relieve pain, manage stress, or address other health concerns.[5] The needles are made using different materials such as stainless steel or stainless steel coated with gold, copper, or silver.[47] The most used material is stainless steel due to its durability and low cost, while gold is often preferred for patients with metal sensitivities. Although it was possible to use stainless steel acupuncture microneedles to prepare K^+ ISEs with Nernstian behavior in the concentration range between 10^{-4} and 10^{-1} M KCl (see the Supporting Information), we chose for most experiments to use gold-coated microneedles and covered these with a monolayer of 1-hexanethiol[48] to minimize chances of forming a water layer at the needle surface, which could contribute to potential drifts. The formation of a water layer may be promoted by the hydrophilicity of the substrate surface, polar groups on the surfaces of the carbon solid contact and substrate, as well as the strength of adhesion at the interfaces of the ion-selective membrane, the solid contact, and the substrate surface.[49−52] After coating the 160 μm diameter needles with a carbon solid contact layer and an ISM layer, the final ISE diameter was typically in the range from 260 to 360 μm, which corresponds approximately to the diameter of 31−28 gauge needles. Figure S7 shows images of the uncoated and coated needles.

Ion-Selective Electrode Behavior. *K^+-ISEs.* To investigate the influence of pore architecture (pore size distribution, pore accessibility) of the different carbons as solid contacts in microneedle based ISEs, electrodes with MCN, CIM carbon, and SPC solid contact layers were prepared, and their responses as K^+-ISEs were compared (Table 3). ISEs with all three types of carbon function well and give close to Nernstian slopes with linear responses between log a_{K^+} values of −4.5 to −1.0, as shown in Figure 4a,b. This covers the normal range in clinical samples (3.4−5.3 mM).[53,54] Anything lower than 2.5 mM[55] is considered severe hypokalemia, and higher than 6 mM[56] corresponds to severe hyperkalemia. Electrode resistances are all in the range from 2−4 MΩ. We note that the E^0 values vary with the type of carbon; so far we do not understand the source of the difference, and further efforts to investigate this effect are ongoing. The sensors exhibit high selectivity, with selectivity coefficients log $K^{pot}_{K^+,Na^+} \approx -4$ for all three types of carbons (Figure S10a,b), consistent with the high selectivity provided by the ionophore.[57] It is important to note that there is no significant difference between the selectivities of sensors made with each of the carbon materials, which suggests that there is no significant extent of adsorption of free ionophore onto the three types of carbon.[58,59]

Additional hydrophobic protection against water layer formation was provided by adding an alkylthiol monolayer on the gold-coated stainless-steel microneedles. In functioning electrodes, no water layers were observed even after immersion of the electrodes in aqueous K^+ solutions for more than 10 days.

Magnitudes of long-term drift values over a period of a week (days 4−10 in Figure 4c) are between 60 and 227 $\mu V\ h^{-1}$ after a larger initial drift during conditioning of the electrodes. In contrast with our initial hypothesis, given the needle-to-needle variation, no statistical difference was observed for drift values obtained with the three different carbon materials. In all cases, based on measured specific capacitance values of the carbon materials, the amounts of carbon present on the microneedles should have been sufficient, to keep drift within acceptable error limits required for a 1-week period without the need for recalibration (Table 1, see also the Supporting Information). Given that specific capacitances of the three carbons and their pore architectures are very different but drift values overlap, we conclude that the carbon porosity may not be the limiting factor responsible for the drift in these microneedle electrodes. Other potential causes for drift include adsorption of ion-selective membrane components (ionophore, ionophore complexes, ionic sites) on the high surface area carbon

https://doi.org/10.1021/acsami.4c07683
ACS Appl. Mater. Interfaces 2024, 16, 44428−44439

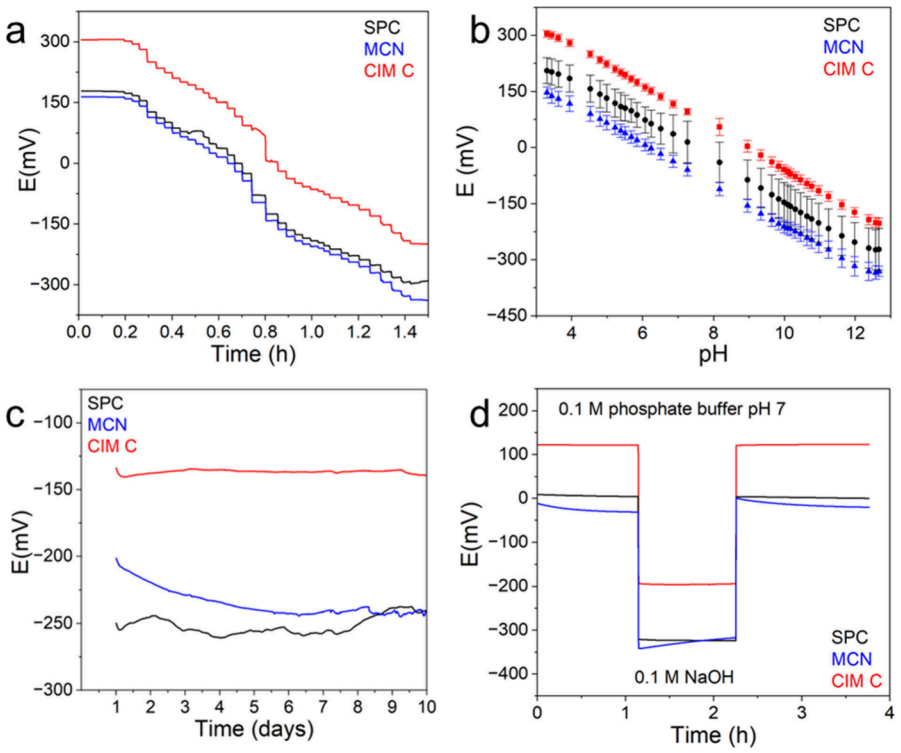

Figure 6. (a) Dynamic responses, (b) calibration curves, (c) long-term drift and (d) water layer test for microneedle ISEs made using SPC (black), MCN (blue) and CIM C (red) as solid contact together with a H^+ ion-selective membrane. (a), (b), and (d) were measured vs a double junction Ag/AgCl reference electrode, whereas (c) was measured vs an electrolytically coated Ag/AgCl wire. The response analyses and water layer tests were carried out after the long-term drift measurements.

materials,[60] swelling of the polymer membrane and the heterogeneous carbon-containing layer with time due to water uptake, changes in the composition of the ion-selective membrane due to leaching of membrane components into solution, and redox reactions of the carbon surfaces during the measurement.

Maximum drifts for K^+-ISEs that conform to an acceptable error of ±0.3 mM are 59 μV h^{-1} over 1 day or 118 μV h^{-1} over 12 h before recalibration are required (see the Supporting Information). While the drift values obtained with the microneedle ISEs are greater than those reported for nanoporous carbon solid contacts with conventional electrode bodies, the current drift values fall within the stability range needed for a long surgical operation or monitoring concentrations during a short hospital stay.

Oxygen, carbon dioxide, and light sensitivities have been reported to influence electrode performance. In the presence of a water layer between the ISM and solid contact, carbon dioxide can change the local pH, resulting in increased potential drift. All three carbons show negligible response to oxygen (Figure 5a). A small response to CO_2 was observed for the CIM carbon-coated microneedle ISEs (1.0 ± 1.2 mV) and MCN-coated microneedles (−1.0 ± 0.7 mV) (Figure 5a). Also, none of the carbon materials used as the solid contacts were affected by light, indicating that the responses of these sensors are not photosensitive (Figure S11).

pH-ISEs. The gold microneedle ISEs were adapted for pH sensing by using tridodecylamine as the ionophore in the ISM. The electrodes gave near-Nernstian responses of −56.9 ± 0.5 mV/decade for CIM carbon, − 54.7 ± 4.1 mV/decade for MCN, and −55.9 ± 3.1 mV/decade for SPC, with linear responses between pH values of 4.5 and 11.2, as shown in Figure 6a,b. The average E^0 values differ with the type of carbon used, and resistances range from 0.3−0.7 MΩ, lower than for K^+-ISEs. The response time is less than 10 s. The pH-ISEs also exhibit high selectivity, with log $K^{pot}_{H^+,Na^+} \approx -12$ for all three types of carbon (Figure S10c,d), as expected for the use of this ionophore.

The long-term potential stability of these pH sensors was measured by exposing the ISEs to phosphate buffer solution over 10 days, and the potential drift was measured from days 4−10, as shown in Figure 6c. The average drift for electrodes with MCN solid contacts is similar to that for the corresponding K^+-sensing electrodes, while that for electrodes with SPC is slightly greater. In contrast, the potential drift for pH electrodes using CIM carbon as solid contact is significantly lower (~20 μV h^{-1}), which means that these electrodes can be used to obtain measurements within the acceptable error (±0.04) for at least 2 days without the need for recalibration. This improvement may be related to the higher specific capacity and better accessibility of the internal pore area in these large-mesopore, high-surface-area materials for ionophore complexes or ionic sites. Limitations related to the polymeric membrane appear to be less of an influence with the pH ISMs as compared to the K^+ ISMs. Two notable differences between these two PVC-based membranes are the plasticizer (*o*-NPOE vs DOS) and, of course, the ionophores that were used (tridodecylamine vs valinomycin). The CIM carbon-based pH electrodes also have better E^0 reproducibilities from needle to needle than those prepared with MCN or SPC. No water layer was observed for SPC and CIM C microneedle electrodes (Figure 6d). MCN showed a slight positive drift when switching the solutions from the phosphate buffer to NaOH and upon returning to the phosphate buffer

https://doi.org/10.1021/acsami.4c07683
ACS Appl. Mater. Interfaces 2024, 16, 44428−44439

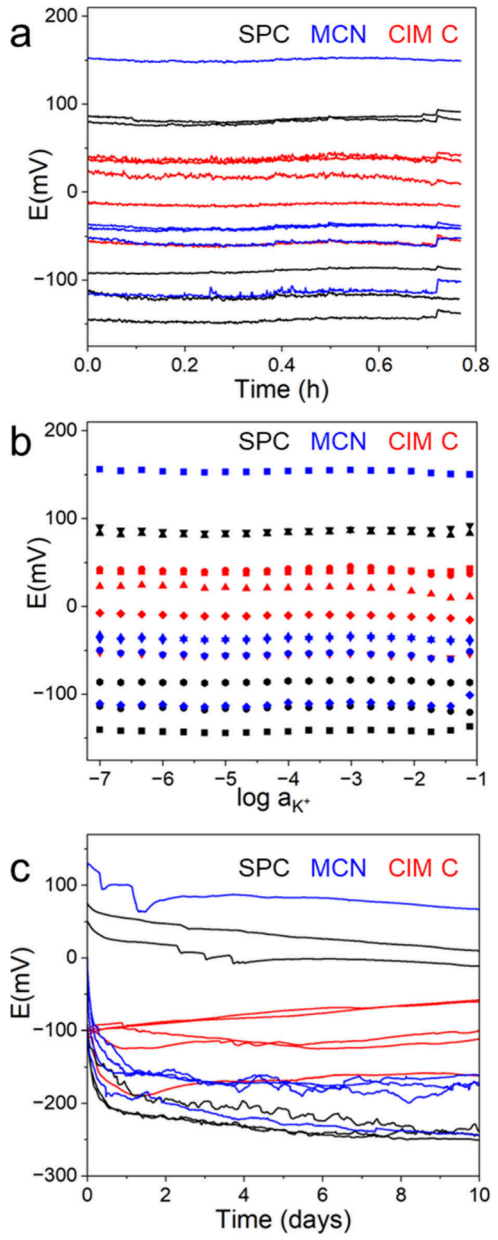

Figure 7. (a) Dynamic responses, (b) calibration curves for potassium ion response, and (c) long-term drift for microneedle REs made using CIM C (red), MCN (blue), and SPC (black) as solid contact and reference membrane.

solution, indicating water layer formation. This may be related to the moderate hydrophilicity observed for MCN (Figure S12). The pH ISEs are not sensitive to oxygen (Figure 5b).

Microneedle Reference Electrode (RE) Behavior. Microneedle REs with all three types of carbon function well. They show average responses of less than 0.7 mV/decade to K^+ ions (Figure 7). Magnitudes of their drift values over a week (days 4−10) are on the order of 100 μV h^{-1}. Average E^0 values for the REs have a wider standard deviation than for the ISEs. Reference electrode resistances are all in the range from 2 to 4 MΩ, similar to the values for the K^+-ISEs. There is no correlation between the resistances and the type of carbon. The reference potential depends on the phase boundary potential of the sample-to-membrane interface, which depends on the ionic liquid slowly leaching out of the membrane.[60−62]

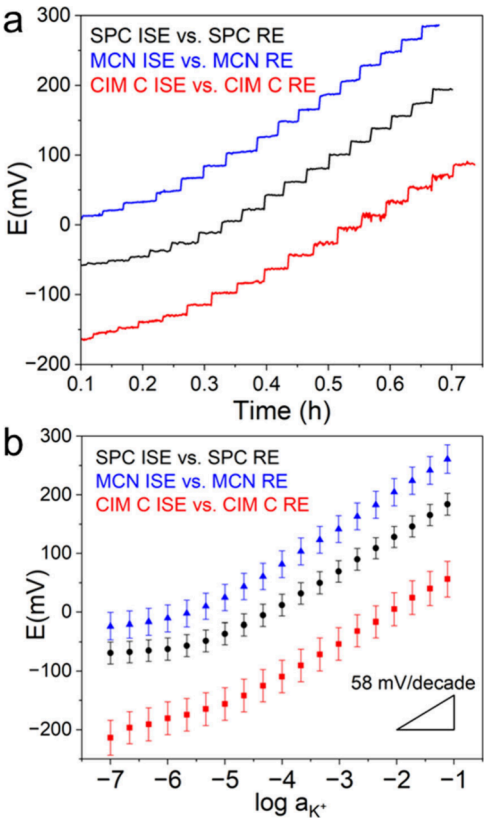

Figure 8. (a) Dynamic responses, and (b) calibration curves for potassium response for microneedle ISEs vs microneedle REs made using MCN (blue), SPC (black), and CIM C (red).

The fact that the REs still functioned after conditioning and long-term stability testing for 10 days implies that the ionic liquid reservoir in the membrane coating on the microneedles was sufficient for this time period.

Combining Microneedle ISEs and REs. Microneedle K^+-ISEs paired with microneedle REs having the same type of carbon as solid contact all function well with near Nernstian responses (Table 3) and linear responses between log a_{K^+} values of −4.5 to −1.0 (Figure 8). For the paired microneedle sensors, average E^0 values were 122 ± 30 mV for CIM C, 250 ± 18 mV for SPC, and 331 ± 24 mV for MCN.

CONCLUSIONS

This study demonstrated that all three carbon materials evaluated here (MCN, CIM carbon, and SPC) are suitable as solid contact materials for microneedle electrodes. Although MCN has the highest specific surface area, most of that surface results from micropores, so that not all components of an ion-selective membrane can penetrate the nanospheres. The mesopore surface area of MCN is slightly higher than the external surface area of nonporous SPC particles, and MCN also had a slightly higher specific capacitance than SPC. In contrast, all ISM components could enter the larger mesopores of CIM carbon, which had a 4−5 times higher mesopore surface area and a 7−9 times higher specific capacitance than the other two carbon materials. We have successfully developed functioning potassium ion and pH sensors that respond linearly in the relevant potassium ion concentration and pH ranges for interstitial fluid using microneedles modified with MCN, CIM carbon, and SPC as solid contact materials.

https://doi.org/10.1021/acsami.4c07683
ACS Appl. Mater. Interfaces 2024, 16, 44428−44439

Even though the potential drifts of these microneedle electrodes are higher than those for nonminiaturized ISEs with the corresponding solid contact materials, their values are comparable to or lower than those reported previously for microneedle ISEs with carbon nanotubes as solid contact (Table S4). The drift values fall within the stability range needed for a long surgical operation or monitoring concentrations during a short hospital stay. There is no significant difference in the potential drift measured using the three different carbon materials for K^+-ISEs in spite of their different pore architectures. This suggests that the observed potential drift values for these microneedle electrodes are also affected by factors other than the pore architecture of the carbon solid contact. Adsorption of ion-selective membrane components on the high surface area carbon materials, swelling of the polymer membrane with time due to water take-up, changes in the composition of the ion-selective membrane due to leaching of membrane components into solution, or redox reactions of the carbon surfaces during the measurement may also contribute to the drift. It is notable though that in the case of pH-ISEs, CIM carbon, with its highest specific capacitance, largest mesopores, and full accessibility of pores to components of the ion-selective membrane, was the best solid-contact material among those investigated here, giving an excellent potential stability of 30 $\mu V\ h^{-1}$. Taken together, these results emphasize the importance of considering not only the solid contact material when optimizing sensor drift, but also the other membrane components.

■ ASSOCIATED CONTENT

Supporting Information

The Supporting Information is available free of charge at https://pubs.acs.org/doi/10.1021/acsami.4c07683.

Additional experimental details, electrochemical data, considerations of solid-contact mass requirements, K^+ sensing with stainless steel microneedles, repairing imperfections in the ISMs, and selectivity data (PDF)

■ AUTHOR INFORMATION

Corresponding Authors

Philippe Bühlmann − *Department of Chemistry, University of Minnesota, Minneapolis, Minnesota 55455, United States;* orcid.org/0000-0001-9302-4674; Email: buhlmann@umn.edu

Andreas Stein − *Department of Chemistry, University of Minnesota, Minneapolis, Minnesota 55455, United States;* orcid.org/0000-0001-8576-0727; Email: a-stein@umn.edu

Authors

Yevedzo Chipangura − *Department of Chemistry, University of Minnesota, Minneapolis, Minnesota 55455, United States*

Maria Komal − *Department of Chemistry, University of Minnesota, Minneapolis, Minnesota 55455, United States*

Vilma S. M. Brandao − *Department of Chemistry, University of Minnesota, Minneapolis, Minnesota 55455, United States;* orcid.org/0000-0003-4592-4162

Christopher Sedmak − *Department of Chemistry, University of Minnesota, Minneapolis, Minnesota 55455, United States*

Jung Suk Choi − *Department of Chemistry, University of Minnesota, Minneapolis, Minnesota 55455, United States*

Sarah L. Swisher − *Department of Electrical and Computer Engineering, University of Minnesota, Minneapolis, Minnesota 55455, United States*

Complete contact information is available at: https://pubs.acs.org/10.1021/acsami.4c07683

Notes

The authors declare the following competing financial interest(s): A.S., P.B., and the University of Minnesota (UMN) have a patent and a patent application (U.S. patent no. 9,874,539; US2020/059979) relating to the use of CIM carbon in ion-selective and reference electrodes. The UMN and the inventors are entitled to standard royalties should licensing revenue be generated from these inventions.

■ ACKNOWLEDGMENTS

This work was partially supported by funding from the Industrial Partnership for Research in Interfacial and Materials Engineering (IPRIME-NMP) and from an InterS&Ections grant by the College of Science and Engineering at the University of Minnesota. The authors acknowledge the International Institute for Biosensing (IIB) at the University of Minnesota for providing seed funds that contributed to the research results reported within this paper. Parts of this work were carried out at the Characterization Facility, University of Minnesota, which receives partial support from the NSF through the MRSEC (Award Number DMR-2011401) and the NNCI (Award Number ECCS-2025124) programs. We thank Dr. Xin I. N. Dong for obtaining XPS spectra and Brian D. Spindler for providing the SEM image of CIM carbon and for insightful discussions.

■ REFERENCES

(1) Heikenfeld, J.; Jajack, A.; Feldman, B.; Granger, S. W.; Gaitonde, S.; Begtrup, G.; Katchman, B. A. Accessing Analytes in Biofluids for Peripheral Biochemical Monitoring. *Nat. Biotechnol.* **2019**, *37* (4), 407−419.

(2) Imani, S.; Bandodkar, A. J.; Mohan, A. M. V.; Kumar, R.; Yu, S.; Wang, J.; Mercier, P. P. A Wearable Chemical−Electrophysiological Hybrid Biosensing System for Real-Time Health and Fitness Monitoring. *Nat. Commun.* **2016**, *7* (1), No. 11650.

(3) Lyzwinski, L.; Elgendi, M.; Shokurov, A. V.; Cuthbert, T. J.; Ahmadizadeh, C.; Menon, C. Opportunities and Challenges for Sweat-Based Monitoring of Metabolic Syndrome via Wearable Technologies. *Commun. Eng.* **2023**, *2*, No. 48.

(4) Ming, D. K.; Jangam, S.; Gowers, S. A. N.; Wilson, R.; Freeman, D. M. E.; Boutelle, M. G.; Cass, A. E. G.; O'Hare, D.; Holmes, A. H. Real-Time Continuous Measurement of Lactate Through a Minimally Invasive Microneedle Patch: A Phase I Clinical Study. *BMJ. Innov.* **2022**, *8* (2), 87−94.

(5) Oh, J.; Jang, S. G.; Moon, S.; Kim, J.; Park, H. K.; Kim, H. S.; Park, S. M.; Jeong, U. Air-Permeable Waterproofing Electrocardiogram Patch to Monitor Full-Day Activities for Multiple Days. *Adv. Healthc. Mater.* **2022**, *11* (12), No. 2102703.

(6) Park, H.; Park, W.; Lee, C. H. Electrochemically Active Materials and Wearable Biosensors for the In Situ Analysis of Body Fluids for Human Healthcare. *NPG Asia Mater.* **2021**, *13*, No. 23.

(7) Sempionatto, J. R.; Lasalde-Ramírez, J. A.; Mahato, K.; Wang, J.; Gao, W. Wearable Chemical Sensors for Biomarker Discovery in the Omics Era. *Nat. Rev. Chem.* **2022**, *6* (12), 899−915.

(8) Parrilla, M.; Cuartero, M.; Padrell Sánchez, S.; Rajabi, M.; Roxhed, N.; Niklaus, F.; Crespo, G. A. Wearable All-Solid-State Potentiometric Microneedle Patch for Intradermal Potassium Detection. *Anal. Chem.* **2019**, *91* (2), 1578−1586.

(9) Parrilla, M.; Ortiz-Gómez, I.; Cánovas, R.; Salinas-Castillo, A.; Cuartero, M.; Crespo, G. A. Wearable Potentiometric Ion Patch for On-Body Electrolyte Monitoring in Sweat: Toward a Validation Strategy to Ensure Physiological Relevance. *Anal. Chem.* **2019**, *91* (13), 8644−8651.
(10) Li, H.; Wu, G.; Weng, Z.; Sun, H.; Nistala, R.; Zhang, Y. Microneedle-Based Potentiometric Sensing System for Continuous Monitoring of Multiple Electrolytes in Skin Interstitial Fluids. *ACS Sens.* **2021**, *6* (6), 2181−2190.
(11) Parrilla, M.; Vanhooydonck, A.; Johns, M.; Watts, R.; De Wael, K. 3D-Printed Microneedle-Based Potentiometric Sensor for pH Monitoring In Skin Interstitial Fluid. *Sens. Actuators B Chem.* **2023**, *378*, No. 133159.
(12) Molinero-Fernandez, Á.; Wang, Q.; Xuan, X.; Konradsson-Geuken, Å.; Crespo, G. A.; Cuartero, M. Demonstrating the Analytical Potential of a Wearable Microneedle-Based Device for Intradermal CO_2 Detection. *ACS Sens.* **2024**, *9* (1), 361−370.
(13) Dervisevic, M.; Dervisevic, E.; Esser, L.; Easton, C. D.; Cadarso, V. J.; Voelcker, N. H. Wearable Microneedle Array-based Sensor for Transdermal Monitoring of pH levels in Interstitial Fluid. *Biosens. Bioelectron.* **2023**, *222*, No. 114955.
(14) Hu, J.; Stein, A.; Bühlmann, P. Rational design of all-solid-state ion-selective electrodes and reference electrodes. *TrAC, Trends Anal. Chem.* **2016**, *76*, 102−114.
(15) Bakker, E.; Bühlmann, P.; Pretsch, E. Carrier-Based Ion-Selective Electrodes and Bulk Optodes. 1. General Characteristics. *Chem. Rev.* **1997**, *97* (8), 3083−3132.
(16) Hu, J.; Zou, X. U.; Stein, A.; Bühlmann, P. Ion-Selective Electrodes with Colloid-Imprinted Mesoporous Carbon as Solid Contact. *Anal. Chem.* **2014**, *86* (14), 7111−7118.
(17) Shao, Y.; Ying, Y.; Ping, J. Recent Advances in Solid-Contact Ion-Selective Electrodes: Functional Materials, Transduction Mechanisms, and Development Trends. *Chem. Soc. Rev.* **2020**, *49*, 4405−4465.
(18) Rousseau, C. R.; Bühlmann, P. Calibration-Free Potentiometric Sensing with Solid-Contact Ion-Selective Electrodes. *TrAC, Anal. Chem.* **2021**, *140*, No. 116277.
(19) Cheong, Y. H.; Ge, L.; Lisak, G. Highly Reproducible Solid Contact Ion Selective Electrodes: Emerging Opportunities for Potentiometry - A Review. *Anal. Chim. Acta* **2021**, *1162*, No. 338304.
(20) Bao, H.; Ye, J.; Zhao, X.; Zhang, Y. Conductive Polymer Nanoparticles as Solid Contact in Ion-Selective Electrodes Sensitive to Potassium Ions. *Molecules* **2023**, *28* (7), No. 3242.
(21) Mazzaracchio, V.; Serani, A.; Fiore, L.; Moscone, D.; Arduini, F. All-Solid State Ion-Selective Carbon Black-Modified Printed Electrode for Sodium Detection in Sweat. *Electrochim. Acta* **2021**, *394*, No. 139050.
(22) Paczosa-Bator, B. All-solid-state Selective Electrodes using Carbon Black. *Talanta* **2012**, *93*, 424−427.
(23) Ozer, T.; Henry, C. S. All-Solid-State Potassium-Selective Sensor Based on Carbon Black Modified Thermoplastic Electrode. *Electrochim. Acta* **2022**, *404*, No. 139762.
(24) Rousseau, C. R.; Chipangura, Y. E.; Stein, A.; Bühlmann, P. Effect of Ion Identity on Capacitance and Ion-to-Electron Transduction in Ion-Selective Electrodes with Nanographite and Carbon Nanotube Solid Contacts. *Langmuir* **2024**, *40* (3), 1785−1792.
(25) Parrilla, M.; Cánovas, R.; Jeerapan, I.; Andrade, F. J.; Wang, J. A Textile-Based Stretchable Multi-Ion Potentiometric Sensor. *Adv. Healthc. Mater.* **2016**, *5* (9), 996−1001.
(26) Parrilla, M.; Ferré, J.; Guinovart, T.; Andrade, F. J. Wearable Potentiometric Sensors Based on Commercial Carbon Fibres for Monitoring Sodium in Sweat. *Electroanalysis* **2016**, *28* (6), 1267−1275.
(27) Soliman, M. A.; Mahmoud, A. M.; Elzanfaly, E. S.; Abdel Fattah, L. E. Design and Application of Supramolecular Based Solid-Contact Ion-Selective Electrode for Selective Green Determination of Tenofovir Disoproxil Fumarate. *Int. J. Electrochem. Sci.* **2024**, *19* (2), No. 100477.
(28) Ye, J.; Li, F.; Gan, S.; Jiang, Y.; An, Q.; Zhang, Q.; Niu, L. Using sp2-C dominant porous carbon sub-micrometer spheres as solid transducers in ion-selective electrodes. *Electrochem. Commun.* **2015**, *50*, 60−63.
(29) Jiang, Z.; Xi, X.; Qiu, S.; Wu, D.; Tang, W.; Guo, X.; Su, Y.; Liu, R. Ordered mesoporous carbon sphere-based solid-contact ion-selective electrodes. *J. Mater. Scie.* **2019**, *54* (21), 13674−13684.
(30) Lai, C.-Z.; Fierke, M. A.; Stein, A.; Bühlmann, P. Ion-Selective Electrodes with Three-Dimensionally Ordered Macroporous Carbon as the Solid Contact. *Anal. Chem.* **2007**, *79* (12), 4621−4626.
(31) Li, Z.; Jaroniec, M. Colloidal Imprinting: A Novel Approach to the Synthesis of Mesoporous Carbons. *J. Am. Chem. Soc.* **2001**, *123* (37), 9208−9209.
(32) Fierke, M. A.; Lai, C. Z.; Bühlmann, P.; Stein, A. Effects of Architecture and Surface Chemistry of Three-Dimensionally Ordered Macroporous Carbon Solid Contacts on Performance of Ion-Selective Electrodes. *Anal. Chem.* **2010**, *82* (2), 680−688.
(33) Hu, J.; Stein, A.; Bühlmann, P. A Disposable Planar Paper-Based Potentiometric Ion-Sensing Platform. *Angew. Chem., Int. Ed.* **2016**, *55* (26), 7544−7547.
(34) Anderson, E. L.; Chopade, S. A.; Spindler, B.; Stein, A.; Lodge, T. P.; Hillmyer, M. A.; Bühlmann, P. Solid-Contact Ion-Selective and Reference Electrodes Covalently Attached to Functionalized Poly(ethylene terephthalate). *Anal. Chem.* **2020**, *92* (11), 7621−7629.
(35) Hu, J.; Zhao, W.; Bühlmann, P.; Stein, A. Paper-Based All-Solid-State Ion-Sensing Platform with a Solid Contact Comprising Colloid-Imprinted Mesoporous Carbon and a Redox Buffer. *ACS Appl. Nano Mater.* **2018**, *1* (1), 293−301.
(36) United States Code of Federal Regulations §493.931 [Title 42, Chapter IV, Subchapter G, Part 493 *Laboratory requirements*, Subpart 931 *Routine chemistry*], 2024, https://www.ecfr.gov/current/title-42/chapter-IV/subchapter-G/part-493, accessed on June 12, 2024.
(37) Teymourian, H.; Tehrani, F.; Mahato, K.; Wang, J. Lab under the Skin: Microneedle Based Wearable Devices. *Adv. Healthc. Mater.* **2021**, *10* (17), No. 2002255.
(38) Tehrani, F.; Teymourian, H.; Wuerstle, B.; Kavner, J.; Patel, R.; Furmidge, A.; Aghavali, R.; Hosseini-Toudeshki, H.; Brown, C.; Zhang, F.; et al. An Integrated Wearable Microneedle Array for the Continuous Monitoring of Multiple Biomarkers in Interstitial Fluid. *Nat. Biomed. Eng.* **2022**, *6* (11), 1214−1224.
(39) Fang, Y.; Gu, D.; Zou, Y.; Wu, Z.; Li, F.; Che, R.; Deng, Y.; Tu, B.; Zhao, D. A Low-Concentration Hydrothermal Synthesis of Biocompatible Ordered Mesoporous Carbon Nanospheres with Tunable and Uniform Size. *Angew. Chem., Int. Ed.* **2010**, *49* (43), 7987−7991.
(40) Palaka, E.; Grandy, S.; Darlington, O.; McEwan, P.; van Doornewaard, A. Associations Between Serum Potassium and Adverse Clinical Outcomes: A Systematic Literature Review. *Int. J. Clin. Pract.* **2020**, *74* (1), No. e13421.
(41) Bard, A. J.; Faulkner, L. R.; White, H. S. *Electrochemical Methods: Fundamentals and Applications*; Wiley: 2022.
(42) Meier, P. C. Two-Parameter Debye-Hückel Approximation for the Evaluation of Mean Activity Coefficients of 109 Electrolytes. *Anal. Chim. Acta* **1982**, *136*, 363−368.
(43) Oesch, U.; Simon, W. Lifetime of neutral carrier based ion-selective liquid-membrane electrodes. *Anal. Chem.* **1980**, *52* (4), 692−700.
(44) Bakker, E.; Pretsch, E.; Bühlmann, P. Selectivity of Potentiometric Ion Sensors. *Anal. Chem.* **2000**, *72* (6), 1127−1133.
(45) Choi, K. R.; Chen, X. V.; Hu, J.; Bühlmann, P. Solid-Contact pH Sensor with Covalent Attachment of Ionophores and Ionic Sites to a Poly(decyl methacrylate) Matrix. *Anal. Chem.* **2021**, *93* (50), 16899−16905.
(46) Chipangura, Y. E.; Spindler, B. D.; Bühlmann, P.; Stein, A. Design Criteria for Nanostructured Carbon Materials as Solid Contacts for Ion-Selective Sensors. *Adv. Mater.* **2024**, *36*, No. 2309778.
(47) Li, Y.; Han, H.; Pan, D.; Zhang, P. Fabrication of a Micro-Needle Sensor Based on Copper Microspheres and Polyaniline Film

for Nitrate Determination in Coastal River Waters. *J. Electrochem. Soc.* **2019**, *166* (12), B1038−B1043.
(48) Zou, X. U.; Cheong, J. H.; Taitt, B. J.; Bühlmann, P. Solid Contact Ion-Selective Electrodes with a Well-Controlled Co(II)/Co(III) Redox Buffer Layer. *Anal. Chem.* **2013**, *85* (19), 9350−9355.
(49) Fibbioli, M.; Morf, W. E.; Badertscher, M.; de Rooij, N. F.; Pretsch, E. Potential Drifts of Solid-Contacted Ion-Selective Electrodes Due to Zero-Current Ion Fluxes Through the Sensor Membrane. *Electroanalysis* **2000**, *12* (16), 1286−1292.
(50) Hambly, B.; Guzinski, M.; Pendley, B.; Lindner, E. Evaluation, Pitfalls and Recommendations for the "Water Layer Test" for Solid Contact Ion-selective Electrodes. *Electroanalysis* **2020**, *32* (4), 781−791.
(51) De Marco, R.; Veder, J.-P.; Clarke, G.; Nelson, A.; Prince, K.; Pretsch, E.; Bakker, E. Evidence of a Water Layer in Solid-Contact Polymeric Ion Sensors. *Phys. Chem. Chem. Phys.* **2008**, *10* (1), 73−76.
(52) Veder, J.-P.; De Marco, R.; Clarke, G.; Chester, R.; Nelson, A.; Prince, K.; Pretsch, E.; Bakker, E. Elimination of Undesirable Water Layers in Solid-Contact Polymeric Ion-Selective Electrodes. *Anal. Chem.* **2008**, *80* (17), 6731−6740.
(53) Hutter, T.; Collings, T. S.; Kostova, G.; Karet Frankl, F. E. Point-of-Care and Self-Testing for Potassium: Recent Advances. *Sens. Diagn.* **2022**, *1* (4), 614−626.
(54) Hirsch, J. S.; Parikh, R.; Richardson, S.; Bock, K. R.; Sakhiya, V.; Fishbane, S.; Jhaveri, K. D. Serum Potassium Laboratory Reference Ranges Influence Provider Treatment Behaviors for Hyperkalemia. *Nephrol. Dial. Transplant.* **2021**, *36* (3), 563−565.
(55) Mark, J.; Jenny, C. Hypokalaemia: Improving the investigation, management and therapeutic monitoring of hypokalaemic medical inpatients at a district general hospital. *BMJ. Qual. Improv. Rep.* **2015**, *4* (1), No. u209049.w203670.
(56) Rosano, G. M. C.; Tamargo, J.; Kjeldsen, K. P.; Lainscak, M.; Agewall, S.; Anker, S. D.; Ceconi, C.; Coats, A. J. S.; Drexel, H.; Filippatos, G.; et al. Expert consensus Document on the Management of Hyperkalaemia in Patients with cardiovascular Disease Treated with Renin Angiotensin Aldosterone System Inhibitors: Coordinated by the Working Group on Cardiovascular Pharmacotherapy of the European Society of Cardiology. *Eur. Heart J. Cardiovasc. Pharmacother.* **2018**, *4* (3), 180−188.
(57) Bühlmann, P.; Pretsch, E.; Bakker, E. Carrier-Based Ion-Selective Electrodes and Bulk Optodes. 2. Ionophores for Potentiometric and Optical Sensors. *Chem. Rev.* **1998**, *98* (4), 1593−1688.
(58) Spindler, B. D.; Graf, K. I.; Dong, X. I. N.; Kim, M.; Chen, X. V.; Bühlmann, P.; Stein, A. Influence of the Composition of Plasticizer-Free Silicone-Based Ion-Selective Membranes on Signal Stability in Aqueous and Blood Plasma Samples. *Anal. Chem.* **2023**, *95* (33), 12419−12426.
(59) Kim, M.; Dong, X. I. N.; Spindler, B. D.; Bühlmann, P.; Stein, A. Functionalizing Carbon Substrates with a Covalently Attached Cobalt Redox Buffer for Calibration-Free Solid-Contact Ion-Selective Electrodes. *Anal. Chem.* **2024**, *96*, 7558−7565.
(60) Dong, X. I. N.; Spindler, B. D.; Kim, M.; Stein, A.; Bühlmann, P. Spontaneous Mesoporosity-Driven Sequestration of Ionic Liquids from Silicone-Based Reference Electrode Membranes. *ACS Sens.* **2023**, *8* (4), 1774−1781.
(61) Zhang, T.; Lai, C.-Z.; Fierke, M. A.; Stein, A.; Bühlmann, P. Advantages and Limitations of Reference Electrodes with an Ionic Liquid Junction and Three-Dimensionally Ordered Macroporous Carbon as Solid Contact. *Anal. Chem.* **2012**, *84* (18), 7771−7778.
(62) Kakiuchi, T.; Yoshimatsu, T.; Nishi, N. New Class of Ag/AgCl Electrodes Based on Hydrophobic Ionic Liquid Saturated with AgCl. *Anal. Chem.* **2007**, *79* (18), 7187−7191.

https://doi.org/10.1021/acsami.4c07683
ACS Appl. Mater. Interfaces 2024, 16, 44428−44439